Cement & Concrete Composites 33 (2011) 474–484

Contents lists available at ScienceDirect

Cement & Concrete Composites

journal homepage: www.elsevier.com/locate/cemconcomp

Experimental observations of early-age drying of Portland cement paste under low-pressure conditions

M. Bakhshi, B. Mobasher *

Department of Civil, Environmental, and Sustainable Engineering, School of Sustainable Engineering and the Built Environment, Arizona State University, Tempe, AZ 85287, USA

ARTICLE INFO

Article history:
Received 23 April 2010
Received in revised form 12 January 2011
Accepted 29 January 2011
Available online 4 February 2011

Keywords:
Cement paste
Cracking
Evaporation
Fiber
Moisture diffusivity
Shrinkage

ABSTRACT

Plastic shrinkage cracking of concrete surfaces directly affects the long-term durability of structures. It can be attributed to the rapid rate of surface moisture evaporation while the microstructure is undergoing the early phases of hydration. A test method for characterizing evaporation parameters and simulating the sequential formation of shrinkage cracks in two-dimensional cement paste samples under low-pressure condition was developed. Effects of sample size, w/c ratio, initial curing and fiber content on weight loss and evaporation rates were investigated. Results indicate that drying occurs in two stages: a constant drying rate period (stage I) and a falling drying rate period (stage II). Vapor diffusion in stage I and unsaturated flow within porous medium in stage II determine the rate of evaporation. Results of diffusivity analysis shows that moisture diffusivity in stage I is higher than its value in stage II by more than one order of magnitude. Crack surface morphology using image analysis on plain and fiber reinforced cement pastes shows significant effect of fiber on controlling plastic shrinkage cracks.

1. Introduction

Plastic shrinkage cracks in concrete reduce load carrying capacity, and accelerate deterioration, resulting in increased maintenance costs and reduced service life [1,2]. These cracks are the main routes through which aggressive agents such as chloride ions penetrate into the concrete mass and threaten the long-term durability of structures [3]. Plastic shrinkage in presence of restraints leads to tensile stresses which may easily exceed the low tensile strength of fresh concrete and result in cracking. Although attributed to several driving forces such as differential settlement, thermal dilation, and autogenous deformation [4], plastic shrinkage cracking in concrete occurs principally due to a high rate of water evaporation from the concrete surface [5–7].

Several test methods have been implemented using fans [8–10], fans and heaters [11,12], or heat lamps [13] to simulate severe evaporation conditions causing plastic shrinkage cracks in fresh concrete. Wind tunnel [14] and vacuum drying [15] have also been used to expedite the drying process. However, these tests were not designed to focus on evaporation characteristics of the drying material as the principal driving force of plastic shrinkage. Also, results of test methods in which the drying of fresh concrete have been studied lack accurate measurement of the evaporation rate and data interpretation based on transport characteristics. While Wongtanakitcharoen and Naaman [16] and Wang et al. [17] studied the effect of fiber content, w/c ratio, and fly ash on normalized cumulative moisture loss using fan, heater, and methanol treatment respectively, parameters addressing rates of evaporation were not utilized in their work. Samman et al. [18] used an electric fan to investigate the effect of w/c ratio, admixtures, and silica fume on the normalized cumulative moisture loss and maximum rate of evaporation. However, maximum rate of evaporation is not sufficient to characterize different materials characteristics. Berhane [19] evaluated the effect of w/c ratio and ambient relative humidity using evaporation rates obtained from moisture loss curves. However, the scale of data requires the evaporation rates to be interpreted based on mass transport parameters. Hall and Hoff [20] analyzed the drying of clay brick ceramics using two distinct stages: a constant drying rate period and a falling drying rate period. They then extended the results from porous media to stones and concrete. Analysis of the evaporation rates of cement-based materials with direct attention to stages of drying process has not been thoroughly investigated.

Evaporation is viewed as the diffusion of water molecules through the boundary layer at the surface to maintain the equilibrium of liquid–gas phase transition [21–26]. During the drying phase, moisture flows through the porous material toward the evaporative surface to supply the necessary surface flux. The relationship between unsaturated flow within concrete pores and evaporation rate on the surface can be used to measure moisture diffusivity [27,28]. By analyzing moisture loss data during the

* Corresponding author. Tel.: +1 480 965 0141; fax: +1 480 965 0557.
E-mail address: Barzin@asu.edu (B. Mobasher).

0958-9465/$ - see front matter © 2011 Elsevier Ltd. All rights reserved.
doi:10.1016/j.cemconcomp.2011.01.009

drying of well hydrated cement paste samples, Garbalińska used desorptive measurement techniques to determine moisture diffusivity [29]. A Similar analytical method is proposed to measure moisture diffusivity in drying fresh cement pastes.

Plastic shrinkage cracks due to a high rate of evaporation are two-dimensional [30]. However, a majority of recent publications have focused on one-dimensional cracking of the concrete by utilizing special restraints [4–6,12,31]. Characterization of images taken from a drying surface helps in understanding crack initiation, propagation, and stabilization during the drying process.

A test method to monitor the drying of fresh cement paste and the formation of plastic two-dimensional cracks is presented in this work. This test method allows measuring material properties that characterize mass transfer during the early stages of fresh paste drying. A drying technique based on a low-pressure condition was employed to cause a rapid rate of evaporation while weight loss was measured. This drying method imposes a one-dimensional moisture flow through the thickness and facilitates parameter estimation from the mass transfer data. The test method was applied to a variety of samples in order to evaluate the impact of sample thickness, surface area, w/c ratio, duration of initial curing and fiber content on the evaporation characteristics being tested. An analytical method to determine moisture diffusivity using experimental data is presented and the effects of different testing parameters on diffusion coefficients are investigated. The development of crack patterns during drying is documented using time-lapse photography. The images have been used to determine the ability of the fibers in controlling shrinkage cracking in drying cement pastes.

2. Testing methodology

Apparatus of the developed low-pressure drying test method is shown in Fig. 1a. A prismatic sample is filled with fresh paste such that its face is exposed and all other sides are sealed. The mold consists of interlocking pieces made of polycarbonate as shown in Fig. 1b and uses anchor hooks to connect the fresh paste with the mold, providing shrinkage restraint in two directions. The sample is placed on a load cell which serves as a digital scale, and the entire assembly is placed inside a glass desiccator. The weight of the sample is continuously monitored throughout the drying cycle. Using a vacuum pump and a pressure regulator the air pressure inside the desiccator is lowered to absolute 1700 Pa (0.5 in Hg) and maintained at this pressure throughout the test. This level of air pressure was selected as a system level parameter after extensive pressure calibration procedures. If the pressure is too low, evaporation occurs at normal rates, and if it is too high, microstructural damage due to cavitation occurs. A controlled test condition therefore requires evaporation rates which simulate the range of severe atmospheric conditions. A condensing system including a D-Drying apparatus is used similar to Copeland and Hayes [32] to remove the water vapor from the desiccator. Similar preliminary results from comparison of the weight of the condensed water in the flask with the total moisture loss at the end of the test show the efficiency of the condensing system. The weight loss measured was recorded using a computer interface unit. The specimen surface was photographed at 15 min intervals using a digital camera mounted 10 cm above the sample. To avoid excessive moisture removal at the beginning of the test, a calibration procedure was developed using a cement paste exposed to several vacuum pressures such that the rate of evaporation was maintained at a constant rate. Based on this procedure, a test procedure consisting of 30 min at 34 kPa (10 in Hg), followed by a decrease in pressure to 1700 Pa (0.5 in Hg) for the remainder of the test was selected. The test procedure was subjected to an additional calibration using liquid water as the evaporating material. This indicated the free water evaporation rate of the test setup.

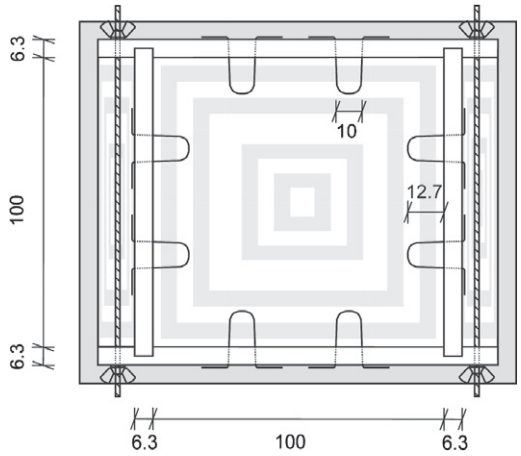

Fig. 1b. Plan view of the mold (numbers in mm).

3. Analysis of typical evaporation data under low-pressure test condition

3.1. Cumulative moisture loss and evaporation rate versus time

The cumulative moisture loss curve was obtained for periods of up to 24 h or more, and adjusted by means of a baseline calibration curve. Cumulative moisture loss data were subjected to a numeri-

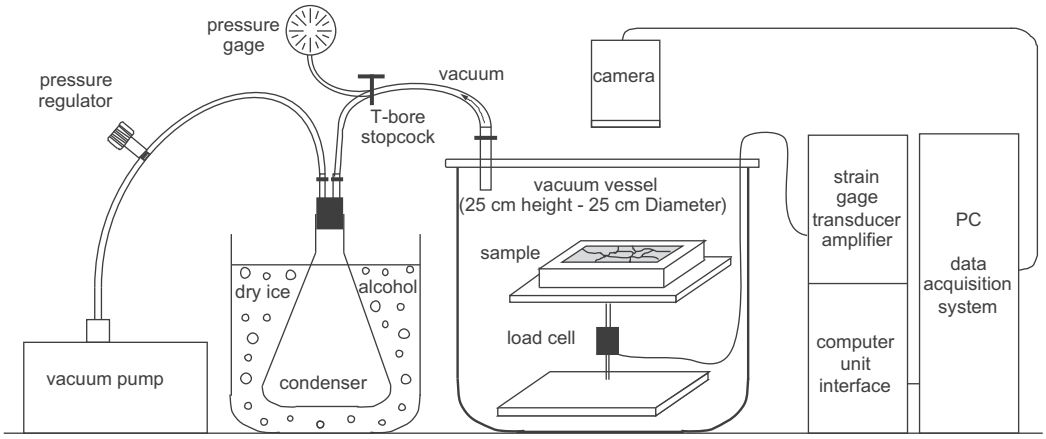

Fig. 1a. Schematic of vacuum drying test setup.

cal differentiation procedure in order to measure the evaporation rate. Results were expressed with respect to the exposed surface area in accordance to:

$$J = \frac{\Delta M}{A\Delta t} = \frac{1}{A}\frac{dM}{dt} \quad (1)$$

where J is the evaporation rate (kg/m^2 s), ΔM is the mass change at specified time steps (kg), Δt is the time step (s) and A is the surface area of the original sample (m^2).

Cumulative moisture loss and evaporation rate curves for a typical cement paste sample are shown in Fig. 2a. Under constant drying condition, the drying rate of cement paste at the beginning is roughly constant with an evaporation rate of 0.42 kg/(m^2 h) during first 10 h, and gradually reduces to 0.05 kg/(m^2 hr) afterwards. This change in the evaporation rate is also presented in log format. Fig. 2b shows the evaporation rate versus log of drying time which is in accordance with results obtained by Hall et al. [33], Cooling [34] for clay brick ceramics, and Kowalski [35] for wet capillary-porous materials such as paper, leather, ceramics and clay. Similar to their observations, drying of cement pastes under constant external conditions occurs in two distinct stages of a constant drying rate period (stage I), and a falling drying rate period (stage II).

Different stages of drying can be described based on the degree of continuity between liquid and vapor phases. Schematics of state phases and moisture transport during drying process of porous media according to Scherer [36] and Plumb et al. [37] are presented in Fig. 3. As shown in Fig. 3a and 3b, during stage I drying, the main phase transitions occur at the boundary surface and vapor phase diffusion into the air is determining rate of evaporation. Hall and Hoff [20] referred to several experimental data showing that stage I behavior is independent of capillary processes inside the material. Drying rate at early time is constant and about the same as rate of evaporation from water surface exposed to the same conditions [4,33]. This was verified by the evaporation tests on water samples. Results of water surface evaporation compared with a plain cement paste sample are shown in Fig. 4. Both samples show evaporation rates in the range of 0.45 kg/(m^2 h). It is therefore postulated that within stage I drying, a continuous liquid phase is present in the pore structure and external evaporative flux away from the surface causes a gradient in capillary pressure in the pores which is the main mechanism of liquid migration from inside toward the boundary [38]. Note that visible plastic cracks were seen as early as 3 h as shown in Fig. 5, and fully developed up to 4 h, a time period well within the stage I drying. Since in this stage, drying takes place under external mass transfer control, potential cracking could have no significant effect in increasing evaporation rate which was the same before and after cracking.

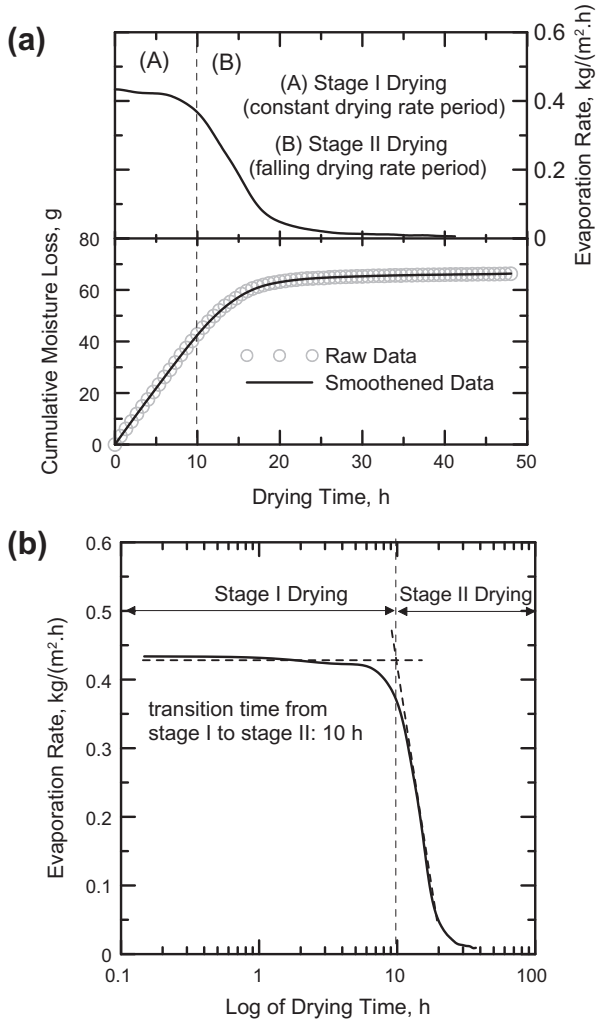

Fig. 2. Typical cumulative moisture loss and evaporation rate of a cement paste sample versus time, (a) in linear scale, (b) in log scale.

As the liquid phase water moves to the surface and evaporates with a constant rate during stage I drying, the moisture content drops continuously. The moisture content at the surface reaches a critical value at and below which the material is unable to support the necessary flux to the surface to satisfy the potential evaporation [39]. At this time, stage II drying begins and rate of evaporation starts to fall. Referring to the results presented in Fig. 2b, this transition in drying stage is gradual. An empirical definition of transition time is defined by the intersection point of two asymptotic linear approximations to the evaporation rate data at stage I and stage II. As shown in Fig. 2b, this transition time for a plain cement paste sample is determined as 9.7 h. Fig. 3c shows that in stage II drying, the liquid phase becomes discontinuous while vapor phase becomes continuous within the matrix. Therefore, phase transitions take place within capillary pores and mass transfer begins to occur through the pore vapor phase. Thus, unsaturated capillary flow determines the rate of evaporation and drying happens under internal mass transfer control [39]. In stage II drying, the removal of moisture is mainly controlled by diffusion which dominates the capillary forces [40]. During this period, the moisture content decreases slowly until it reaches the equilibrium value below which the material cannot be dried.

3.2. Calculation of moisture diffusivity

Evaporation from water surface can be treated as a boundary layer problem, in which the water vapor diffuses from a saturated state on the surface to the ambient moisture concentration [21–26]. Rate of evaporation is controlled by two parameters of binary air–water vapor diffusivity and the concentration gradient. Evaporation from a fresh cement paste at stage I is quite similar to the case of clay, ceramics, and other capillary porous media [41]. It consists of a boundary layer identical to water evaporation boundary, and an unsaturated flow for transfer of liquid water from within the material to supply the flux. The focus of this work is on calculation of diffusivity of water within the cement paste rather than air–water vapor diffusivity at the boundary layer. The calculated diffusivities at stage I and II show the potential for moisture conductivity through the fresh cement paste.

Flow within the porous medium can be described by the extended Darcy equation for unsaturated flow [33,38] which in the case of a one-dimensional expression is written as:

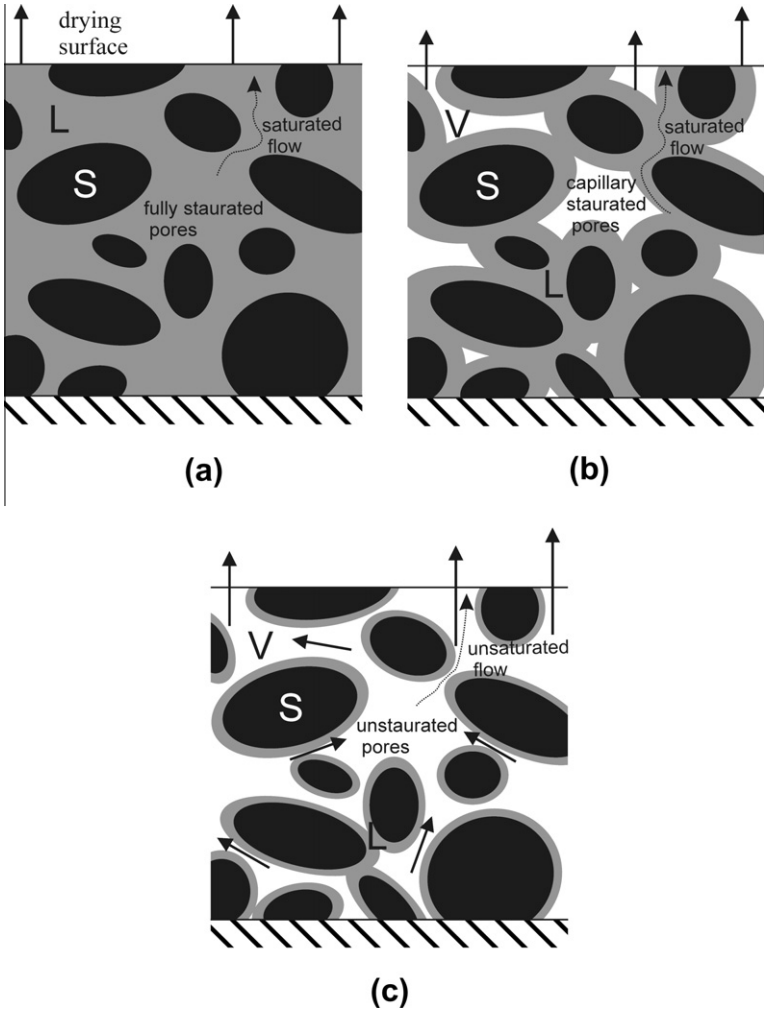

Fig. 3. Schematics of moisture transport during drying process of porous media representing solid (S), liquid (L) and vapor phases (V): (a) initial condition (full saturation), (b) capillary saturation (continuous liquid phase), (c) hygroscopic state (continuous vapor phase).

$$\frac{\partial \theta}{\partial t} = \frac{\partial}{\partial x}\left(K\frac{\partial \psi}{\partial x}\right) \tag{2}$$

where θ is the volume fraction moisture content (–), ψ is the hydraulic or capillary potential (m), K is moisture conductivity (m/s), x is the pass of moisture transfer (m), and t is the time (s).

Definition of capillary diffusivity (m^2/s) as $D = K(\partial\psi/\partial\theta)$ leads us to Fick's second law of diffusion which governs a majority of moisture transfer problems in porous media [15,42,43].

$$\frac{\partial C}{\partial t} = D\frac{\partial^2 C}{\partial x^2} \tag{3}$$

where C is the moisture concentration (kg/m^3), D is the moisture (liquid and vapor) diffusion coefficient (m^2/s) and t is the time (s).

In order to simulate the drying test results using a dual-stage drying concept, two different boundary conditions at the top surface are required. For the first stage, boundary condition of constant flux at the surface can be applied which is obtained directly from experimental data. Boundary condition for the second stage which is a constant concentration at the surface is set to ambient moisture concentration. At ambient pressure of 1 atm, the water vapor pressure is the product of relative humidity and the saturated water vapor pressure. However, in this low-pressure test condition, the sum of the partial pressure of all the species in the air including dry air and water vapor is 1700 Pa. Assuming the percentage of water vapor remains the same after running the vacuum pump, water vapor pressure can be estimated as 2% of barometric pressure which is 34 Pa. The corresponding moisture content defined as $\omega = M_{water}/M_{Dry\ Air} = 0.622 \times P_{water}/(1700\text{-}P_{water})$ is equal to 0.0127 kg of Water/kg of Air. Therefore, moisture concentration can be assumed to be zero as a reasonable approximation. Using the experimental evaporation rate during stage I drying, and zero moisture concentration at stage II, the two required boundary conditions are:

$$\begin{aligned} &\text{Stage I drying}: \quad \text{at } x = L, \quad J = F_0 \\ &\text{Stage II drying}: \quad \text{at } x = L, \quad C_s = C_* = C_{w,\text{low pressure}} \end{aligned} \tag{4}$$

where x is the pass length of diffusion, measured from the bottom face (m), L is the thickness of sample (m), F_0 is the constant flux in stage I drying ($kg/(m^2\ s)$), and C_* is the ambient moisture concentration (kg/m^3).

Considering C_i as the initial moisture concentration (kg/m^3), the initial boundary condition is

$$t = 0, \quad C = C_i \quad 0 \le x \le L \tag{5}$$

Since the bottom surface is impermeable, the boundary condition at the bottom is

$$\text{at } x = 0, \quad J = -D\frac{\partial C}{\partial x} = 0 \tag{6}$$

The analytical solution of Eq. (3), for the initial and boundary conditions of stage I drying, assuming a constant diffusivity is given by Eq. (7) [44].

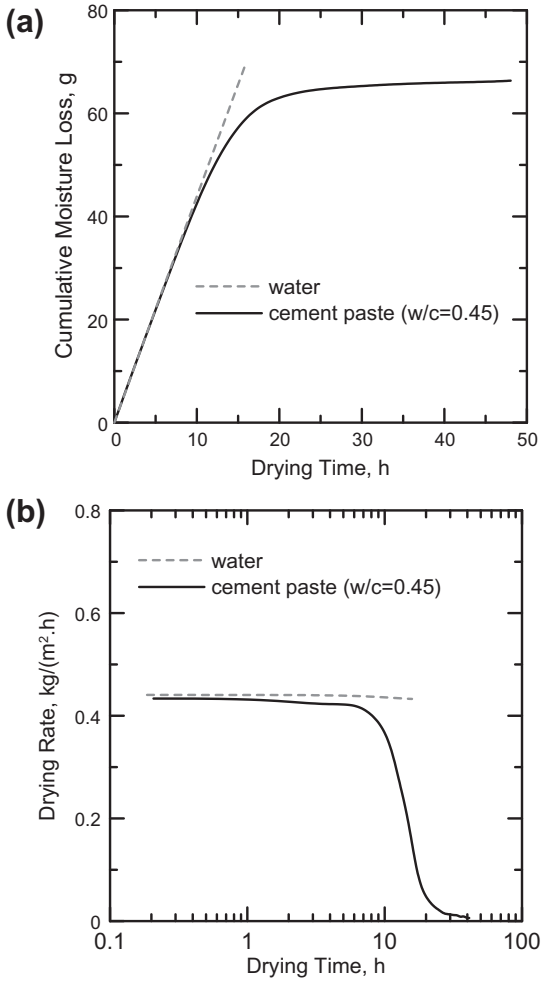

Fig. 4. Results of evaporation tests from water surface comparing to plain cement paste.

$$C(t,x) = C_i + \frac{F_0 L}{D_{\mathrm{I}}}\left\{\frac{D_{\mathrm{I}} t}{L^2} + \frac{3x^2 - L^2}{6L^2} - \frac{2}{\pi^2}\sum_{n=1}^{\infty}\frac{(-1)^n}{n^2} \times \exp\left(\frac{-D_{\mathrm{I}} n^2 \pi^2 t}{L^2}\right)\cos\frac{n\pi x}{L}\right\} \quad (7)$$

where D_{I} is the diffusivity in stage I drying.

Using Eq. (7), moisture concentration at the top surface is obtained providing constant F_0 and D_{I} values. Since stage I drying ends when the surface reaches equilibrium moisture concentration, moisture diffusivity at stage I drying is calculated as long as the time of transition from stage I to stage II has not lapsed. Applying this method on a typical result of a plain cement paste sample results in a diffusivity value as 5.15×10^{-7} m^2/s at stage I drying. Unlike the stage I drying, diffusion coefficients in stage II drying depend on moisture concentration [45]. For simplicity, diffusivity in stage II is taken constant resulting in calculation of an average diffusivity, which is averaged over space and time. Analytical solution for the boundary conditions of stage II drying subjected to constant concentration, C_*, at the surface is [44]:

$$\frac{C - C_i}{C_* - C_i} = 1 - \frac{4}{\pi}\sum_{n=0}^{\infty}\frac{(-1)^n}{2n+1} \times \exp\left\{-D_{\mathrm{II}}(2n+1)^2\pi^2 t/4l^2\right\}\cos\frac{(2n+1)\pi x}{2L} \quad (8)$$

where D_{II} is the diffusivity in stage II drying.

By integrating Eq. (8) over the thickness of sample, total amount of diffusing moisture in stage II drying, which has left the sample at time t, M_t (kg), can be obtained and related to its corresponding quantity after infinite time, M_∞ (kg). Therefore, moisture loss during the advanced phase of drying is given by

$$\frac{M_t}{M_\infty} = 1 - \sum_{n=0}^{\infty}\frac{8}{(2n+1)^2\pi^2}\exp\left\{-D_{\mathrm{II}}(2n+1)^2\pi^2 t/4L^2\right\} \quad (9)$$

Results of analyses performed by Garbalinska [29] on cement-based materials show that in the expansion of Eq. (9), the higher terms with $n > 0$ can be neglected after releasing 40% of the total mass change. As discussed in the following sections, for almost all samples tested in this study, stage II drying begins when more than 60% of the moisture is lost. By considering only first term of the series, moisture diffusivity, D_{II} (m^2/s), can be derived by rearranging Eq. (9) as

$$D_{\mathrm{II}}\frac{\pi^2}{-4L^2} = \frac{\ln\left(1 - \frac{M_t}{M_\infty}\right) - \ln\frac{8}{\pi^2}}{t} \quad (10)$$

Assuming the logarithmic terms on the right hand side of the equation are following a linear relationship with the time, slope of the curve, $a_{\ln}$, can be used to determine moisture diffusivity during stage II drying.

$$\ln\left(1 - \frac{M_t}{M_\infty}\right) - \ln\frac{8}{\pi^2} = a_{\ln} t \quad (11)$$

$$D_{\mathrm{II}} = \frac{-4L^2}{\pi^2}\cdot a_{\ln} \quad (12)$$

Procedures for obtaining the slope, $a_{\ln}$ for a plain cement paste sample is shown in Fig. 6a. This process results in calculation of diffusivity as 3.33×10^{-9} m^2/s at stage II drying. Using calculated values of diffusivity from stage I and stage II drying, total amount of moisture loss at any time can be predicted. Comparison of the simulation and experimental data for a drying cement paste sample is shown in Fig. 6b. This figure shows that dual-stage drying model and corresponding moisture diffusivity values can be used to predict drying characteristics of cement-based materials in this low-pressure condition. Since two different boundary conditions are applied in stage I and stage II, the continuity of the slope is not completely achieved as shown by the slight bump in the simulation data. Further studies on variable diffusion coefficients and applying different boundary conditions such a convective-diffusive boundary condition at stage II are required in order to better fit the results.

Note that the evaporation rate in the normal room pressure is different than that in the low pressure desiccator, where rate of water vapor diffusion in the desiccator controls the rate of vaporization and drying. The reason is that diffusion rates of water vapor in low pressure are much higher than that under normal room pressure, because the diffusion coefficient of gasses is roughly inversely proportional to the gas pressure at constant temperature [46]. Therefore, the calculated diffusion coefficients for stage I and II drying are only representatives for this low-pressure drying condition. However, the analysis is applicable to drying at normal room pressure providing evaporation rates and ambient moisture concentration of that test condition.

4. Experimental program

4.1. Scope of test program

Effects of different variables including sample size, w/c ratio, duration of initial curing, and fiber content were studied. The scope

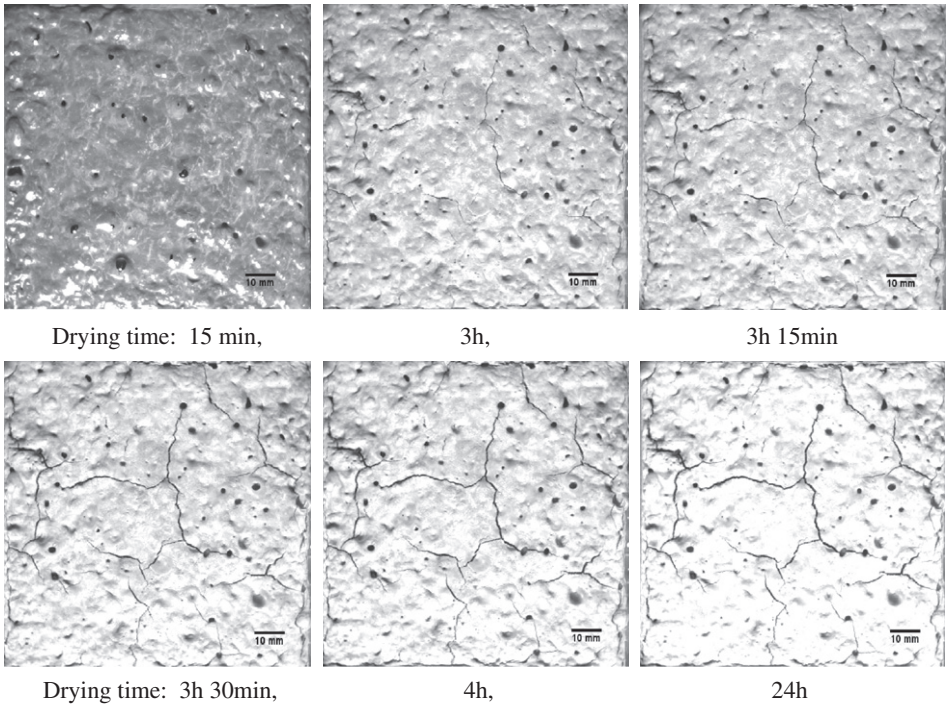

Fig. 5. 2-D crack development during drying of a fresh plain cement paste sample.

of the test program is shown in Table 1 and includes a test matrix consisting of twelve sets of evaporation tests conducted on different portland cement pastes. Variables of the study included sample thickness, surface area, w/c ratio, duration of initial curing and fiber content. Two sample thicknesses of 11 and 21 mm, and two surface dimensions of 127 mm × 127 mm and 100 mm × 100 mm were used. w/c ratios of 0.45, 0.5, 0.55 and 0.6 were chosen as material variables. Effect of fibers was investigated by adding 1.5, 3, 4.5 and 6 kg/m^3 Alkali-Resistant (AR) glass fibers (St. Gobain Vetrotext) to the plain cement paste, equivalent to 0.06%, 0.11%, 0.17% and 0.23% volumetric fractions. Cement paste samples with initial curing of 0, 3 and 24 h were also tested to evaluate effect of curing duration.

4.2. Materials, mixing, placing and curing procedures

The test program consisted of variations in the physical parameters of testing such as sample area, depth, and materials mixture variations. The mixture proportions for cement pastes are provided in Table 2 and include Type I/II portland cement as the primary binding agent. In fiber reinforced cement pastes, Alkali-Resistant (AR) glass fibers of 24 mm in length and aspect ratio of 150 were used. The fibers are multi-fiber strand of 100 round filaments bonded together. The filament diameter is 14 microns and fiber has elastic modulus of 72 GPa, specific gravity of 2.68 and tensile strength of 1700 MPa. After mixing in accordance with ASTM C1116 [47], samples were cast in the molds immediately and subjected to the test within 15 min. No curing was applied except for samples of two test series which were covered with a plastic sheet for 3 and 24 h at the room temperature before running tests.

5. Parameter estimation

Parameters obtained from evaporation tests includes aspects of initial rate of evaporation, time of transition from stage I to stage II drying, evaporation rate at 24 h, cumulative moisture loss at 24 h and moisture diffusivities. Results are compiled in Table 3 and are discussed in the following sections.

5.1. Effect of sample size

Evaporation characteristics of samples with the two different thicknesses and surface areas were studied. Two sample thicknesses of 11 mm and 21 mm in addition to two exposed surface dimensions of 100 mm × 100 mm and 127 mm × 127 mm were used. Cumulative moisture loss and evaporation rates of these test series are shown in Fig. 7. As expected, increasing sample thickness and surface area, increased the cumulative moisture loss at the end of the test. Results indicate a 95% increase in the total moisture loss due to doubling of the thickness. A 66% increase in the total moisture loss was observed as the surface area was increased by 62%. Initial evaporation rates changed slightly from 0.42 kg/(m^2 h) to 0.44 and 0.37 kg/(m^2 h) for thicker sample and sample with larger surface area, respectively. Thicker sample has a slightly higher initial evaporation rate (~4%) and if this is attributed to within sample variation, then the initial evaporation is primarily a surface phenomenon. Larger sample however has a lower evaporation rate by 12% during stage I. The difference may be attributed to the side and edge effects, as in the vacuum evaporation the mass flux is only a function of total pressure gradient and the water vapor diffusion coefficient is not related to the size of evaporative surface [48–50]. Since control and thicker samples have approximately the same initial evaporation rates as shown in Table 3, critical moisture concentration reached later for thicker sample due to higher initial moisture content. Therefore the transition time changes from 9.7 h for control to 18.9 h for the thicker sample. This indicates that the critical moisture concentration was reached after losing 63–65% of the initial moisture content. Similarly, the transition time for larger sample was obtained as 12.8 h which refers to the time when 68% of initial moisture is lost. The values of diffusivity at stage I and stage II drying determined for these three samples are shown in Table 3. Values of moisture diffusivities at stage I drying is within range of 4.91 × 10^{-7}–5.27 × 10^{-7} m^2/s. Moisture dif-

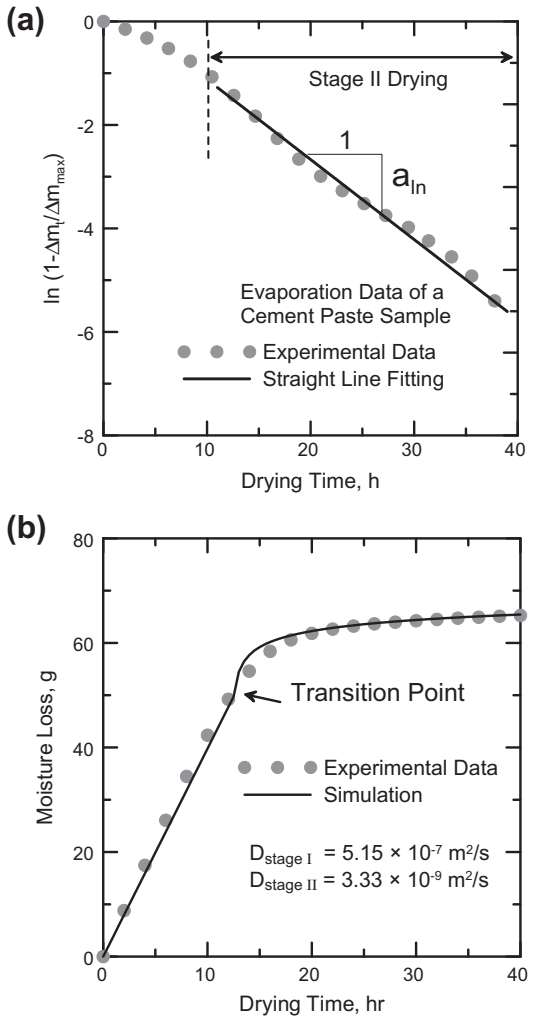

Fig. 6. (a) Deriving a_{ln} by fitting a straight line to the curve of $\ln(1-\Delta M_t/\Delta M_{max})$ versus time in stage II, (b) Simulation of cumulative moisture loss versus experimental data for a cement paste sample.

Table 1
Scope of the test program.

Test series	w/c	Initial curing (h)	Fiber content (kg/m^3)	Thickness (mm)	Surface area (m^2)
P0.45-IC0-F0 (control)	0.45	0	0	11	0.01
P0.45-IC0-F0-Th21	0.45	0	0	21	0.01
P0.45-IC0-F0-SA0.016	0.45	0	0	11	0.016
P0.50-IC0-F0	0.50	0	0	11	0.01
P0.55-IC0-F0	0.55	0	0	11	0.01
P0.60-IC0-F0	0.60	0	0	11	0.01
P0.45-IC3-F0	0.45	3	0	11	0.01
P0.45-IC24-F0	0.45	24	0	11	0.01
P0.45-IC0-F1.5	0.45	0	1.5	11	0.01
P0.45-IC0-F3	0.45	0	3	11	0.01
P0.45-IC0-F4.5	0.45	0	4.5	11	0.01
P0.45-IC0-F6	0.45	0	6	11	0.01

fusivity at stage II is calculated as 3.33×10^{-9} m^2/s for the control sample (P045-IC0-F0), while for thicker (P045-IC0-F0-Th21) and larger (P045-IC0-F0-SA0.016) is determined as 3.6×10^{-9} and 3.25×10^{-9} m^2/s, respectively. Such similar values for moisture diffusivity of portland cement paste mixture validate the range of accuracy of the analytical method.

Table 2
Mix proportions of the test series.

Test series	Portland cement	Water	AR-glass fiber	w/c
P0.45-ICxx-F0*	1450	650	0	0.45
P0.50-IC0-F0	1400	700	0	0.50
P0.55-IC0-F0	1355	745	0	0.55
P0.60-IC0-F0	1310	790	0	0.60
P0.45-IC0-F1.5	1450	650	1.5	0.45
P0.45-IC0-F3	1450	650	3	0.45
P0.45-IC0-F4.5	1450	650	4.5	0.45
P0.45-IC0-F6	1450	650	6	0.45

* This mix proportion was used for P0.45-IC0-F0, P0.45-IC3-F0, P0.45-IC24-F0, P0.45-IC0-F0-Th21 and P0.45-IC0-F0-SA0.016 samples.

5.2. Effect of w/c ratio

Fig. 8a shows the cumulative moisture loss-time curves for water cement ratios of 0.45, 0.5, 0.55 and 0.6 after a 24 h drying period, which range from 0 to 65, 68, 74 and 78 g respectively. As expected, the initial rate of evaporation is rather the same for all samples, however higher w/c ratio resulted in a higher cumulative moisture loss. An increase in w/c from 0.45 to 0.6 led to 20% increase in total moisture loss. On the other hand, initial drying rate as shown in Fig. 8a was slightly affected by increasing w/c ratio. Average rates of evaporation at first drying stage were 0.42, 0.44, 0.45 and 0.46 kg/(m^2 h) for samples with w/c ratio of 0.45, 0.50, 0.55 and 0.60, respectively. These magnitudes are sufficiently close to the rate of evaporation from water surface (i.e. 0.45 kg/(m^2 h)) as the upper limit, hence increasing w/c ratio does not significantly increase the initial evaporation rate. Rates of evaporation at the second drying stage indicate that samples with higher w/c ratios have consistently higher evaporation rates. After 24 h of drying, evaporation rates dropped to 0.03 kg/(m^2 h) for all samples. But the transition time changes from 9.7 h for the series with w/c ratio of 0.45 to 9.8 h, 11 h, and 12.3 h for series with w/c ratios of 0.5, 0.55 and 0.6, respectively. Diffusivity values determined for different w/c ratios are shown in Fig. 8b and indicate that moisture diffusivities of different samples at stage I drying are very similar. However, at stage II drying moisture diffusivities increased by 5%, 21% and 25% when w/c ratio varied from 0.45 to 0.5, 0.55 and 0.6.

5.3. Effect of duration of initial curing

Effect of duration of curing prior to initiation of drying was studied by test series P0.45-IC0-F0, P0.45-IC3-F0 and P0.45-IC24-F0. These samples had the same mix proportions and differed only in duration of initial curing which ranged from 0, to 3, and to 24 h. Fig. 9 shows the results of the cumulative moisture loss and evaporation rates versus time. The cumulative moisture loss after 24 h of drying was substantially reduced by increasing the duration of initial curing. This parameter fell from 65 g for the non-cured cement paste to 49 g and 26 g for cement pastes with initial curing of 3 and 24 h, respectively translating into 24% and 60% reduction in cumulative moisture loss of cement paste. This transition can only be justified by the change of microstructure, pore size distributions and physical properties of the transition layer through which evaporation occurs [49]. Results of stage I drying indicate considerable reduction in initial evaporation rates from a control of 0.42 to 0.39 and 0.34 kg/(m^2 h) for 3 and 24 h-cured samples. However, the reduction of drying rates in second stage of drying is more significant, i.e. after 12 h drying when all three test series were on stage II drying, evaporation rates dropped from 0.3 kg/

Table 3
Initial evaporation rates, transition time, evaporation rate at 24 h, cumulative moisture loss, and diffusivities of tested samples.

Test series	Initial evaporation rate (kg/(m^2 h))	Transition time of drying stages (h)	Evaporation rate at 24 h (kg/(m^2 h))	Cumulative moisture loss at 24 h (g)	Moisture diffusivity at stage I (m^2/s)	Moisture diffusivity at stage II (m^2/s)
P0.45-IC0-F0 (control)	0.42	9.7	0.024	65	5.15E−07	3.33E−09
P0.45-IC0-F0-Th21	0.44	18.9	0.300	127	5.27E−07	3.61E−09
P0.45-IC0-F0-SA0.016	0.37	12.8	0.079	108	4.91E−07	3.25E−09
P0.50-IC0-F0	0.44	9.8	0.031	68	5.27E−07	3.50E−09
P0.55-IC0-F0	0.45	11.0	0.039	74	5.33E−07	4.03E−09
P0.60-IC0-F0	0.46	12.3	0.033	78	5.27E−07	4.16E−09
P0.45-IC3-F0	0.39	7.3	0.017	49	1.94E−07	1.25E−09
P0.45-IC24-F0	0.34	3.0	0.019	26	2.78E−08	2.36E−10
P0.45-IC0-F1.5	0.42	10.0	0.043	64	5.05E−07	3.27E−09
P0.45-IC0-F3	0.41	11.2	0.036	65	5.19E−07	2.64E−09
P0.45-IC0-F4.5	0.40	11.5	0.028	65	5.15E−07	2.22E−09
P0.45-IC0-F6	0.38	11.3	0.087	66	5.11E−07	2.08E−09

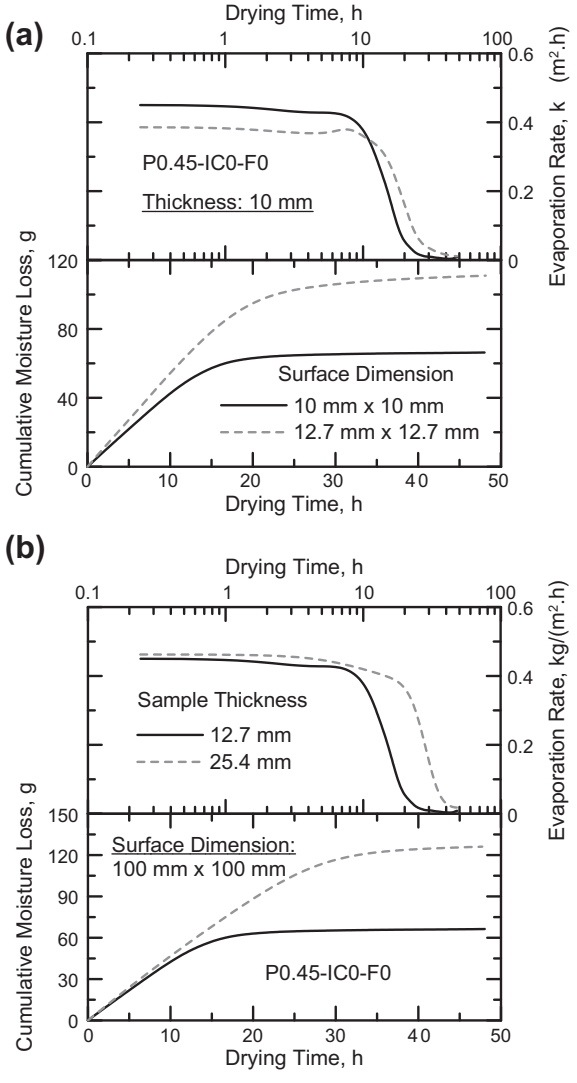

Fig. 7. Effects of surface area and thickness on results of evaporation tests on plain cement paste.

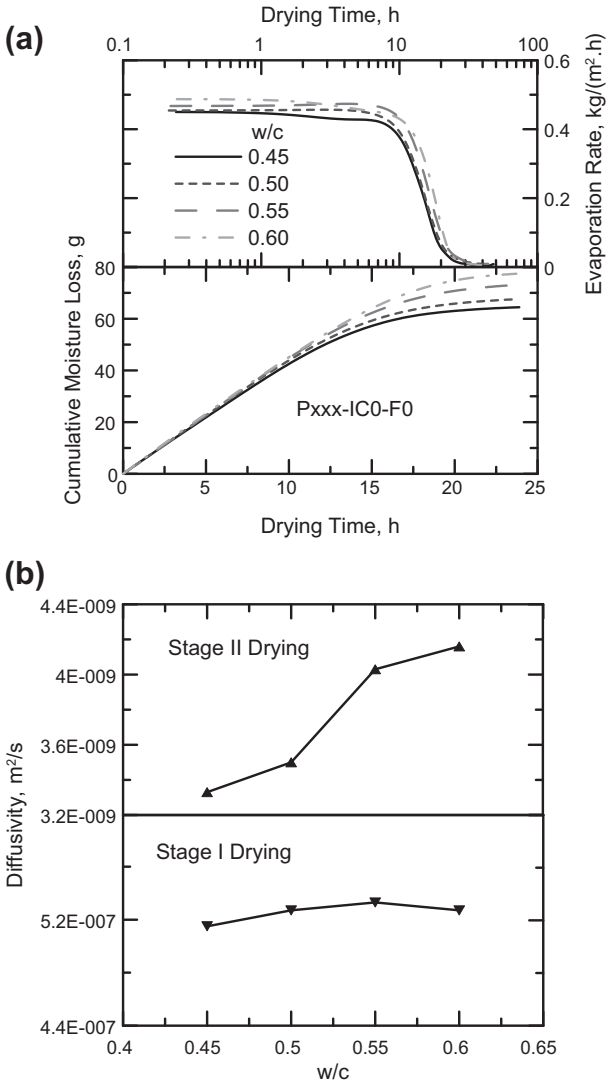

Fig. 8. Effects of w/c ratio on results of evaporation tests on plain cement pastes.

(m^2 h) for control sample to 0.2 kg/(m^2 h) and 0.07 kg/(m^2 h) for 3 h-cured and 24 h-cured samples, respectively. The transition time from stage I to stage II drying decreased from 9.7 h to 7.3 h for the 3 h-cured specimens and down to 3 h for the 24 h-cured sample. The reduction is clearly attributed to the reduction of moisture diffusivities at stage I by increasing curing duration. As shown in Table 3, moisture diffusivity of control sample is 2.7 and 18.5 times than diffusion coefficients of 3 h- and 24 h-cured samples, respectively. Increasing curing duration led to decreasing stage II diffusion coefficient of 3 h-cured and 24 h-cured samples

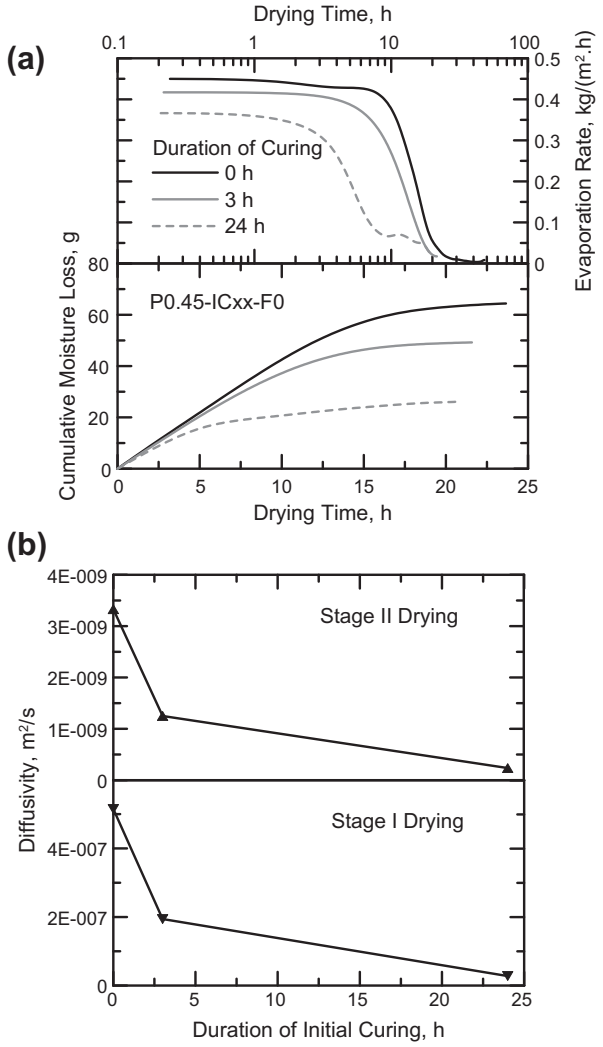

Fig. 9. Effect of curing duration on results of evaporation test on plain cement pastes.

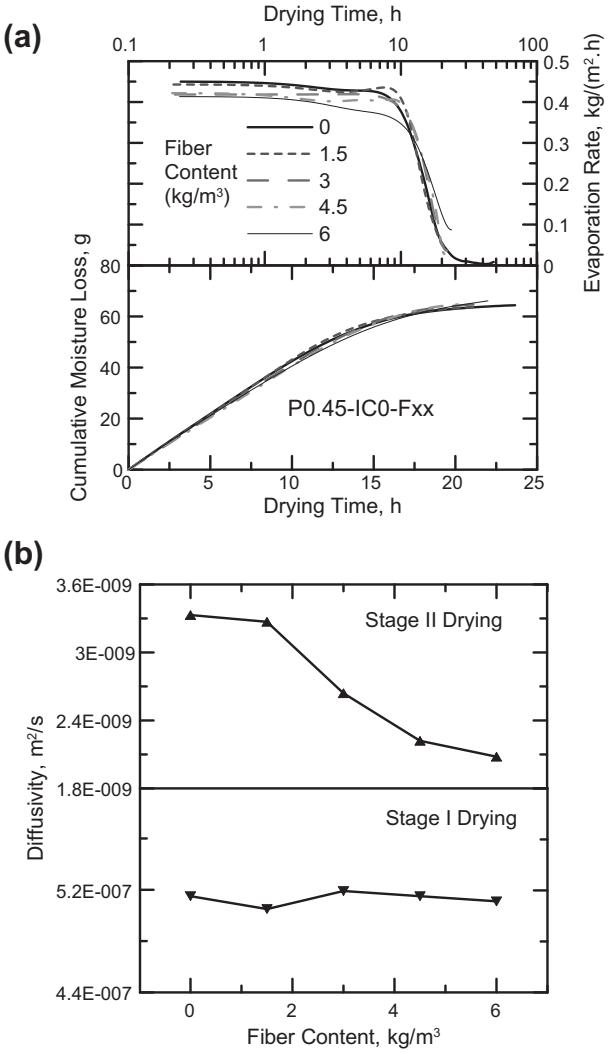

Fig. 10. Results of drying tests on cement paste samples with different content of AR-glass fibers.

comparing to the control sample by as much as 62% and 93%, respectively.

5.4. Effect of fiber content and cracking

Effect of fiber addition and its volume fraction was studied by utilizing AR-glass fiber in the mixture. The effect of fiber reinforcement is compared with the plain cement paste in Fig. 10. Fiber addition to the cement paste did not result in any significant reduction in cumulative moisture loss at the end of the test. This is in agreement with the result of Naaman et al. [12] which shows fibers result in the reduction of the cumulative moisture loss by only 5% or less. However, AR-glass fibers caused slight reduction of evaporation rates at the first drying stage. The initial evaporation rate dropped from 0.42 kg/(m^2 h) for plain sample to 0.42, 0.41, 0.40 and 0.38 kg/(m^2 h) associated with samples with 1.5, 3, 4.5 and 6 kg/m^3 AR-glass fiber additions, respectively. A more significant effect of fiber addition was observed in the manner of transition from the first stage of drying to the second. Addition of fibers resulted in a gradual transition of the modes of drying which could be attributed to the effect of fibers in controlling early-age cracks. As shown in the micrographs of Fig. 11, fiber addition reduced the maximum crack width and cracking area of the cement paste. Since early-age cracks cause the evaporative surface to be more exposed to the low-pressure condition in the desiccator, they may contribute to higher evaporation rates than uncracked surfaces. The transition time from stage I to stage II drying increased by the addition of fiber for all fiber reinforced paste samples to ranges of 10–11.5 h compared to 9.7 h for the control sample.

According to Fig. 10b, diffusivity results at stage I drying do not vary significantly by the change of fiber dosage. Since fiber controls plastic shrinkage cracking during early hours (see Fig. 11), results support the minimal effect of cracks on drying rate in stage I. However, results show a decreasing trend for the diffusivities at stage II by increasing fiber dosage as shown in Fig. 10b. The diffusivities of fiber reinforced cement paste samples with fiber content of 1.5, 3, 4.5 and 6 kg/m^3 are 2%, 20%, 33% and 38% less than corresponding value for plain control sample, respectively. This effect can be explained by the higher degree of surface cracking in the presence of fibers which reduces the mean path length of moisture transfer to reach the surface. The result can thus be interpreted as the effect of cracking on the drying rate in stage II when unlike to stage I, the restraint of cracks by fibers, the increased number of microcracks, and reduced crack widths are effective on lowering moisture diffusivity. This explanation can be supported by the fact that in stage II, drying happens under internal mass transfer control and the microstructure plays a significant role on the drying process. As shown in Fig. 11, 22% and 61% reduction in areal fraction of cracks

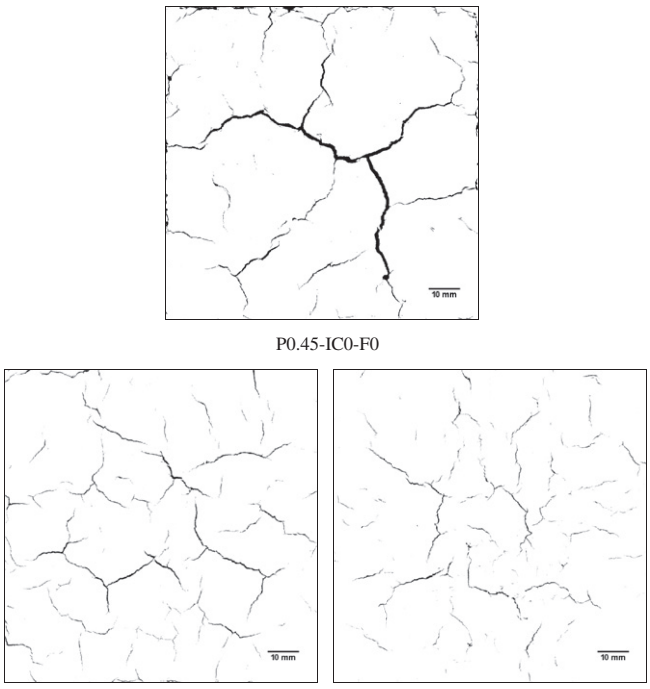

Fig. 11. Crack pattern of cement paste specimens with and without AR-glass fibers after 24 h of drying under low-pressure test condition.

were observed by adding 3 and 6 kg/m^3 fibers to cement paste, respectively. Also, maximum crack widths of samples associated with 3 and 6 kg/m^3 fibers were 47% and 71% less than corresponding value for the control sample, respectively. The length of microcracks however was increased by addition of fibers. Higher moisture diffusivities at stage II in plain pastes with wider cracks compared to fiber reinforced pastes with narrower but more plentiful cracks are in accordance with the studies performed by Bažant and Raftshol [51] and Aldea et al. [52]. While they found the moisture diffusivity and the water permeability are proportional to the crack width cubed, results of another experimental study [53] indicated that diffusivity of concrete increased 2.25 times by shrinkage cracks with a width of 0.1 mm and a spacing of 70 mm. Also, the recent experimental data reported by Vejmelková et al. [54] show that moisture diffusivity of high performance concrete and cement pastes increased by one order of magnitude due to the cracking. In addition, Torrijos et al. [55] reported the increase of water permeability by one order of magnitude due to increase of crack density from 0.25 to 0.45 cm/cm^2. Considering all these results, it can be concluded that fibers reduce moisture diffusivities of cracked samples at stage II by reducing crack width and crack density which results in the durability improvement of cement-based materials.

6. Conclusion

A test method capable of characterizing evaporation parameters and simulating sequential formation of shrinkage cracks in two-dimensional samples under low-pressure condition was developed. The cumulative moisture loss and evaporation rates were calculated. Based on the results of experiments and analyses in this study, following conclusions may be drawn:

1. Drying of cement pastes can be segmented into two distinct stages: constant drying rate period (stage I) and falling drying rate period (stage II). During stage I drying, evaporation rate is constant, main phase transitions take place at the surface and vapor phase diffusion process is rate-determining. At the transition time, moisture content at the surface reaches a critical value. During stage II drying, phase transitions take place within capillary pores and unsaturated capillary flow is rate-determining. During this stage, moisture content decreases slowly until reaching the equilibrium value below which the material cannot be dried.
2. The cumulative moisture loss and evaporation rate curves can be used to differentiate evaporation characteristics of different cement pastes. Parameters including thickness and surface area of samples, w/c ratio, and duration of initial curing have significant effects on evaporation results.
3. A dual-stage drying model based on two different boundary conditions at the top surface and a diffusional moisture transfer within the pores can be used to simulate experimental results. The model can be used to determine moisture diffusivity of the samples during drying process. Moisture diffusivity is higher in stage I by more than one order of magnitude than its values in stage II.
4. Fibers contribute to the control of plastic shrinkage cracks. However, presence of fibers and cracking control do not affect the drying rate in stage I drying. In stage II drying, the presence of fibers reduces the diffusivity values. This could be due to the restraint of cracks by fibers which is effective in stage II when internal mass transfer controls the drying. Results show that 22% and 61% reduction in areal fraction of cracks were observed by adding 3 and 6 kg/m^3 fibers to cement paste, respectively. Also, maximum crack widths of samples associated with 3 and 6 kg/m^3 fibers were 47% and 71% less than corresponding value for the control sample, respectively. Since there is a cubic relationship between permeability rate and the crack width, effect of fibers in controlling the plastic crack width results in significant durability enhancement.
5. Among several different parameters investigated in this study, duration of curing has the most significant effect on the reduction of drying rate and moisture diffusivities.

Acknowledgement

This research was partially funded by support from the Arizona Department of Transportation "ADOT" Project SPR-633, Mr. Christ Dimitroplos, Program Manager. This support is greatly appreciated. The views and opinions of authors expressed herein do not necessarily state or reflect those of the ADOT, or Federal Highway Administration "FHWA". Neither the ADOT nor any of its employees, assumes any legal liability or responsibility for the accuracy, completeness, or usefulness of any information, apparatus, product, or process disclosed in this paper.

References

[1] Kwon SJ, Na UJ, Park SS, Jung SH. Service life prediction of concrete wharves with early-aged crack: probabilistic approach for chloride diffusion. Struct Saf 2009;31(1):75–83.
[2] Huang XM, Yang CY. Early-age concrete cover crack and its effects on concrete cover. Key Eng Mater 2006;302–303:630–6.
[3] Yoon IS, Schlangen E, de Rooij MR, van Breugel K. The effect of cracks on chloride penetration into concrete. Key Eng Mater 2007;348–349:769–72.
[4] Lura P, Pease B, Mazzotta GB, Rajabipour F, Weiss J. Influence of shrinkage-reducing admixtures on development of plastic shrinkage cracks. ACI Mater J 2007;104(2):187–94.
[5] Banthia N, Gupta R. Plastic shrinkage cracking in cementitious repairs and overlays. Mater Struct 2009;42(5):567–79.
[6] Mora-Ruacho J, Gettu R, Aguado A. Influence of shrinkage-reducing admixtures on the reduction of plastic shrinkage cracking in concrete. Cem Concr Res 2009;39(3):141–6.
[7] Cohen MD, Olek J, Dolch WL. Mechanism of plastic cracking in Portland cement and Portland cement–silica fume paste and mortar. Cem Concr Res 1990;20(1):103–19.

[8] Turcry P, Loukili A. Evaluation of plastic shrinkage cracking of self-consolidating concrete. ACI Mater J 2006;103(4):272–9.
[9] Sanjuan MA, Moragues A. A testing method for measuring plastic shrinkage in polypropylene fibre reinforced mortars. Mater Lett 1994;21:239–46.
[10] Nanni A, Ludwig DA, Mcgillis MT. Plastic shrinkage cracking of restrained fiber-reinforced concrete. Transport Res Rec 1993;1382:69–72.
[11] Banthia N, Gupta R. Test method for evaluation of plastic shrinkage cracking in fiber-reinforced cementitious materials. Exp Tech 2007;31(6):44–8.
[12] Naaman AE, Wongtanakitcharoen T, Hauser G. Influence of different fibers on plastic shrinkage cracking of concrete. ACI Mater J 2005;102(1):49–58.
[13] Ma Y, Zhu B, Tan M, Wu K. Effect of Y type polypropylene fiber on plastic shrinkage cracking of cement mortar. Mater Struct 2004;37:92–5.
[14] Jacobsen S, Aarseth LI. Effect of wind on drying from wet porous building materials surfaces – a simple model in steady state. Mater Struct 1999;32:38–44.
[15] Shimomura T, Maekawa K. Analysis of the drying shrinkage behaviour of concrete using a micromechanical model based on micropore structure of concrete. Mag Concr Res 1997;49(181):303–22.
[16] Wongtanakitcharoen T, Naaman AE. Unrestrained early age shrinkage of concrete with polypropylene, PVA, and carbon fibers. Mater Struct 2007;40:289–300.
[17] Wang K, Shah SP, Phuaksuk P. Plastic shrinkage cracking in concrete materials – influence of fly ash and fibers. ACI Mater J 2001;98(6):458–64.
[18] Samman TA, Mirza WH, Wafa FF. Plastic shrinkage cracking of normal and high-strength concrete: a comparative study. ACI Mater J 1996;93(1):36–40.
[19] Berhane Z. Evaporation of water from fresh mortar and concrete at different environmental conditions. ACI J Proc 1984;81(6):560–5.
[20] Hall C, Hoff WD. Water transport in brick, stone, and concrete. New York: Taylor & Francis; 2002.
[21] Sultan E, Boudaoud AI, Amar MB. Evaporation of a thin film: diffusion of the vapour and Marangoni instabilities. J Fluid Mech 2005;543:183–202.
[22] Arya SP. Introduction to micrometeorology. San Diego: Academic Press; 2001.
[23] Huang CH. Pasquill's influence: on the evaporation from various liquids into the atmosphere. J Appl Meteorol 1997;36(8):1021–6.
[24] Brighton PWM. Evaporation from a plane liquid surface into a turbulent boundary layer. J Fluid Mech 1985;159:323–45.
[25] Prata AT, Sparrow EM. Diffusion-driven nonisothermal evaporation. J Heat Transfer 1985;107(1):239–42.
[26] Brutsaert W. A model for evaporation as a molecular diffusion process into a turbulent atmosphere. J Geophys Res 1965;70:5017–24.
[27] Carmeliet J, Hens H, Roels S, Adan O, Brocken H, Cerny R, et al. Determination of the liquid water diffusivity from transient moisture transfer experiments. J Therm Envelope Build Sci 2004;27:277–305.
[28] Janz M. Methods of measuring the moisture diffusivity at high moisture levels. Report TVBM-3076, University of Lund, Lund Institute of Technology. Division of Building Materials; 1997.
[29] Garbalinska H. Application of $\sqrt{t}$-type, logarithmic and half-time methods in desorptive measurements of diffusivity in narrow humidity ranges. Cem Concr Res 2006;36:1294–303.
[30] Mehta PK, Monteiro PJM. Concrete: microstructure, properties and materials. Boston: McGraw-Hill; 2006.
[31] Soroushian P, Ravanbakhsh S. Control of plastic shrinkage cracking with specialty cellulose fibers. ACI Mater J 1998;95(4):429–35.
[32] Copeland LE, Hayes JC. Determination of non-evaporable water in hardened Portland-cement paste. ASTM Bull 1953;194:70–4.
[33] Hall C, Hoff WD, Nixon MR. Water movement in porous building materials – VI. Evaporation and drying in brick and block materials. Build Environ 1984;19(1):13–20.
[34] Cooling LF. Contribution to the study of florescence. II. The evaporation of water from bricks. Trans Brit Ceram Soc 1930;29:39–54.
[35] Kowalski SJ. Thermomechanics of drying processes. New York: Springer; 2003.
[36] Scherer GW. Theory of drying. J Am Ceram Soc 1990;73(1):3–14.
[37] Plumb OA, Gu L, Webb SW. Drying of porous materials at low moisture content. Drying Technol 1999;17(10):1999–2011.
[38] Kowalski SJ. Thermomechanical approach to shrinkage and cracking phenomena in drying. Drying Technol 2001;19(5):731–65.
[39] Garrabrants AC, Kosson DS. Modeling moisture transport from a Portland cement-based material during storage in reactive and inert atmospheres. Drying Technol 2003;21(5):775–805.
[40] Vu TH. Influence of pore size distribution on drying behaviour of porous media by a continuous model. Master of Engineering Dissertation, Otto-von-Guericke-UniversitÃ¤t Magdeburg, Germany; 2006.
[41] Simunek J, Van Genuchten M, Sejna M. The hydrus-1d software package for simulating the one-dimensional movement of water, heat, and multiple solutes in variably-saturated media. Version 3.0, Agriculture Research Service, US Department of Agriculture, Riverside, CA; 2005.
[42] Blandin HP, David JC, Vergnaud JM, Illien JP, Malizewicz M. Modelling of drying of coatings: effect of the thickness, temperature and concentration of solvent. Prog Org Coat 1987;15:163–72.
[43] Hulden M, Hansen CM. Water permeation in coatings. Prog Org Coat 1985;13:171–94.
[44] Crank J. The mathematics of diffusion. New York: Oxford Science Publications; 1989.
[45] Xi Y, Bažant Z, Molina L, Jennings HM. Moisture diffusion in cementitious materials – moisture capacity and diffusivity. Adv Cem Based Mater 1994:1258–66.
[46] Cussler EL. Diffusion: mass transfer in fluid systems. 3rd ed. New York: Cambridge University Press; 2009.
[47] American Society for Testing Materials. Standard Specification for Fiber-Reinforced Concrete, ASTM C1116/C1116M-10. Annual Book of ASTM Standards 2010. Section 4. Construction 04.02.
[48] Tsotsas E, Mujumdar AS. Modern drying technology: computational tools at different scales. Darmstadt, Germany: Wiley-VCH; 2007.
[49] Sebastian P, Turner IW. An investigation of the boundary conditions for a vacuum drying problem – introducing the transition layer concept. Drying Technol 1994;12(4):717–60.
[50] Ramon G, Agnon Y, Dosoretz G. Heat transfer in vacuum membrane distillation: effect of velocity slip. J Membr Sci 2009;331:117–25.
[51] Bažant ZP, Raftshol WJ. Effect of cracking in drying and shrinkage specimens. Cem Concr Res 1982;12:209–26.
[52] Aldea C-M, Shah SP, Karr A. Effect of cracking on water and chloride permeability of concrete. J Mater Civil Eng 1999;11(3):181–7.
[53] Bažant ZP, Sener S, Kim JK. Effect of cracking on drying permeability and diffusivity of concrete. ACI Mater J 1987;84(5):351–8.
[54] Vejmelková E, Padevet P, Cerny. Effect of cracks on hygric and thermal characteristics of concrete. Bauphysik 2008;30(6):438–44.
[55] Torrijos MC, Giaccio G, Zerbino R. Internal cracking and transport properties in damaged concretes. Mater Struct 2010;43:109–21.